Drop Calorimetry Studies on 9Cr–1W–0.23V–0.06Ta–0.09C Reduced Activation Steel

S. Raju · B. Jeya Ganesh · Arun Kumar Rai · S. Saroja · E. Mohandas · M. Vijayalakshmi · Baldev Raj

Abstract The temperature dependence of enthalpy increment ($H_T - H_{298}$) of 9 mass% Cr–1 mass% W–0.23 mass% V–0.06 mass% Ta–0.09 mass% C reduced activation steel has been measured by inverse drop calorimetry in the temperature range 400 K to 1273 K. A critical comparison of present isothermal enthalpy measurements with the results of our previous dynamic calorimetry studies has been made to reveal clearly the occurrence of various diffusional phase transformations that occur at high temperature. These phase changes are marked by the presence of distinct inflections or cusps in an overall nonlinear variation of enthalpy values with temperature. The principal thermal relaxation step of the martensitic microstructure obtained through quenching from the high-temperature γ-austenite phase is observed around 793 K. The ferromagnetic-to-paramagnetic transition of the α-ferrite phase is found to occur at 1015 K. The equilibrium values of γ-austenite start (Ae_1) and finish (Ae_3) temperatures are found to be 1063 K and 1148 K, respectively. A value of 12 J · g^{-1} has been estimated for $\Delta°H^{\alpha \rightarrow \gamma}$ the latent heat associated with the $\alpha \rightarrow \gamma$ transformation. The measured enthalpy increment variation of the α-ferrite phase with temperature has been fitted to a suitable empirical function to estimate the temperature-dependent values of the specific heat. A comparison of the drop calorimetry-based indirect estimate of the specific heat with the direct differential scanning calorimetry-based values revealed that the drop calorimetry estimates are systematically lower than its dynamic calorimetry counterpart. This difference is attributed to the fact that, under finite heating rate conditions that are typical of dynamic calorimetry, measurements

S. Raju (✉) · B. Jeya Ganesh · A. K. Rai · S. Saroja · E. Mohandas · M. Vijayalakshmi · B. Raj
Physical Metallurgy Division, Metallurgy & Materials Group, Indira Gandhi Centre
for Atomic Research (IGCAR), Kalpakkam 603102, India
e-mail: sraju@igcar.gov.in

B. Raj
Indira Gandhi Centre for Atomic Research (IGCAR), Kalpakkam 603102, India

are made under nonequilibrium conditions. Notwithstanding this limitation, there is a good overall agreement between the two C_p values and also among the phase transformation temperatures so that a reliable assessment of thermal properties and phase transformation characteristics of reduced activation steel can be determined by a combined analysis of the results of drop and differential scanning calorimetry.

1 Introduction

It is well known that the availability of reliable and critically assessed thermodynamic data is essential for facilitating the knowledge-driven approach to alloy design [1]. At present, there is an urgent need for generating accurate high-temperature thermochemical and thermophysical property information on many advanced engineering alloys that are slated for applications in conventional and emerging power generation options [2]. The profitable understanding of factors that govern ultimately the materials selection and component design depends to a large extent on our ability to successfully model and simulate the degradation mechanisms that the chosen candidate material is expected to experience during its normal service or under hypothetical accident conditions [1]. While the modelling of materials performance during service is veritably a daunting task when viewed in its entirety of scope and perspective, it is nevertheless useful to address this issue in a compartmentalized manner. The latter modular approach advocates the deployment of simple phenomenological models that are valid at different length scales, with the output stemming from each one of the modules serving as the input needed for exploring the problem at the next higher level of sophistication. In the area of such hierarchical, multi-tiered approach to materials modelling, there has been a sustained effort over the last decade towards developing successful thermodynamic and kinetics protocols that aim at rationalizing or predicting the phase and microstructural stability of advanced engineering materials at the level of classical thermodynamics and continuum mechanics. In such an approach it is difficult to overemphasize the pivotal role played by reliable material property data [1,2].

High-chromium ferritic–martensitic steels containing about 9 mass% 10 mass% Cr with specifically tailored composition limits for minor alloying additions such as Mo, Nb, V, Mn, Ni, Si, N, S, P, etc., are of interest in both conventional and nuclear power generation applications [3] as a result of their attractive combination of physical and mechanical properties, compatibility with liquid metal coolant, and resistance to swelling against fast neutrons [4]. Despite the fact that there have been numerous studies devoted to exploring the microstructure–mechanical property and performance correlation of these materials as a function of several processing variables including melting practices [5–14], there is a relative paucity of experimental data on basic thermodynamic and thermophysical properties. It is in view of this situation that we have undertaken in this study to measure the temperature variation of enthalpy increments of a low-carbon, nuclear-grade 9 mass% Cr-steel containing controlled amounts of W and Ta. The composition of this reduced activation ferritic–martensitic steel (RAFM)

slated for possible application in fusion reactors [3,15] has been designed to minimize the induced radioactivity hazard arising from elements such as Mo, Nb, N, Cu, Co, Al, etc. This is realized by substituting for these elements with comparatively more benign homologous replacements such as W, Ta and V [15]. Recently, the nature of various phase transformations that take place in this steel upon continuous heating has been investigated by us using differential scanning calorimetry [16]. This study, employing inverse drop calorimetry, aims at complementing these results by making accurate enthalpy increment measurements as a function of temperature at close to thermodynamic equilibrium conditions [17].

It is generally understood that static or isothermal drop calorimetry measurements give more accurate values of enthalpy under equilibrium thermodynamic conditions. The dynamic or differential scanning calorimetry studies on the other hand yield data that are obtained under varying degrees of nonequilibrium conditions [17]. As a consequence, dynamic calorimetry-based transformation temperature and transformation enthalpy data require appropriate normalizing to account for finite heating or cooling rate effects [18]. In view of this fact, one of the objectives of this investigation is to make a comparative assessment of equilibrium transformation thermodynamic data obtained in this study using the drop calorimetry technique with the equivalent information obtained using a scanning calorimetry technique [16]. The thermodynamic quantities investigated include the temperature variation of an enthalpy increment and hence specific heat, on-heating transformation temperatures and an estimate of the latent heat associated with the α-ferrite $\rightarrow$ γ-austenite transformation. The relevant experimental details are briefly discussed in the following sections.

2 Experimental Details

2.1 Alloy Preparation and General Characterization

The composition in mass% of the reduced activation steel as determined by optical emission spectroscopy is given as follows: 9.05 Cr, 1.0 W, 0.0036 Mo, 0.50 Si, 0.56 Mn, 0.09 C, 0.0206 N, 0.0036 Al, 0.0043 Co, 0.226 V, 0.005 Cu, 0.0024 Ti, 0.0039 Nb, 0.063 Ta; the balance being Fe. The material is made by vacuum induction melting, followed by vacuum arc refining. In order to minimize the presence of tramp elements that aggravate the induced radioactivity hazard, a fairly pure (99.9 % Fe, 99.5 % Ta, 99.5 % W; 99.9 % Cr, $Fe_{80}V_{20}$ ferrovanadium master alloy, nuclear-grade graphite as the carbon source) starting feed has been used in making the master alloy. The ingot is processed by hot forging and hot rolling into plates with a finish temperature of about 1323 K (1050 °C). In this study, the steel is given an additional solution heat treatment at 1523 K (1250 °C) for about 30 min followed by quenching to room temperature. This solutionizing temperature is somewhat higher than that usually employed, namely, 1323 K (1050 °C), since the presence of highly cohesive Ta and W containing carbides necessitated a higher solutionizing temperature for their complete dissolution in high-temperature γ-austenite phase. But it must be added that, depending on the actual duration of this solutionizing treatment, a small quantity of the δ-ferrite phase is also found to be present in some samples [16].
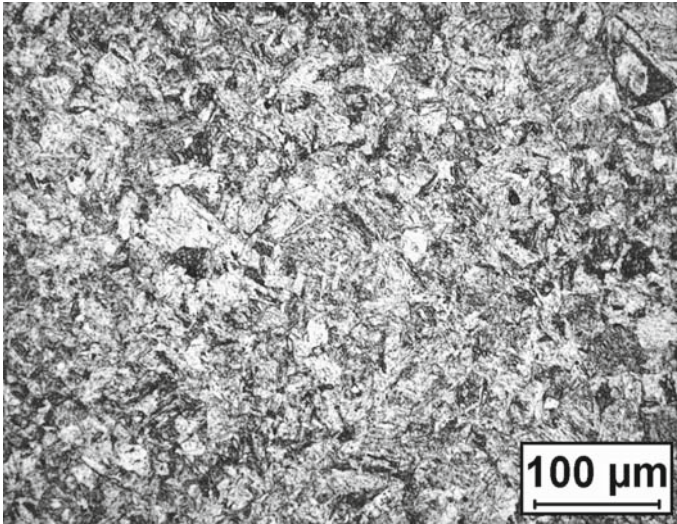
Fig. 1 Optical micrograph of the reduced activation steel in the quenched condition showing lath martensite

An optical micrograph of the typical solution-treated and water-quenched sample is shown in Fig. 1. The copious presence of fine lath martensite is readily apparent. The average microhardness of the martensite microstructure measured with 100 g load is found to vary between 470 and 510 on the Vickers scale. The room temperature ($\sim$293 K) lattice parameter of the α-ferrite phase determined by X-ray diffraction using CuKα radiation is found to be (0.2876 ± 0.003) nm. The bulk density of the sample, as determined using the standard immersion method, is found to be 7.67×10^3 kg $\cdot$ m^{-3}. Using this bulk density value and the X-ray lattice parameter, the average atomic weight of this steel is estimated to be $0.0548(5)$ kg $\cdot$ mol^{-1}.

2.2 Inverse Drop Calorimetry

The inverse drop calorimetry measurements were performed using a Setaram Multi HTC 96$^{\circledR}$ calorimeter in the drop mode. The description of the equipment, calibration (Caluire, France) of heat flux into effective enthalpy and data analysis procedures have been presented in detail in our previous publications and therefore are not elaborated upon here [19,20]. The experiment in its essence consists of instantaneously dropping a sample kept at a fixed reference temperature (T_O) to a well-equilibrated pure alumina bed, maintained at the desired experimental temperature (T) to within ± 0.1 K. The alumina bed is located well within the isothermal zone of a resitively heated graphite furnace. Presuming negligible heat loss to surroundings (other than the analysis chamber), the perturbation in the thermal equilibrium of the drop-bed results in a sudden drop of its temperature, followed by a gradual rise with respect to time to its initial or preset temperature value. By measuring accurately this time (t)–temperature change (ΔT) profile and calibrating it in terms of a similar response arising from the drop of a known mass of reference or calibration standard under iden-

tical experimental conditions, it is possible to quantify the heat flux (area under the $t-\Delta T$ curve in terms of an enthalpy increment [19]. The area under the $t-\Delta T$ curve is determined using an ITC Setaram electronic integrator. The furnace temperature is monitored by a Pt(10 %Rh)/Pt thermopile that is also located in the isothermal zone of the furnace. The differential heat flux calorimetric detector is basically a thermocouple that monitors the difference in temperature between the alumina bed in the upper portion and the empty alumina crucible at the bottom. The thermocouple is calibrated using pure melting point standards of high-purity Zn, Al and Cu which are supplied by Setaram. The error in temperature measurements does not exceed ± 1 K over the temperature range under study.

A typical data collection time of about 20 min to 30 min is maintained in this study. Considering the small mass ((50 to 70) ± 0.1) mg of the sample, this time is considered adequate to ensure the attainment of thermal equilibrium in the experiment. A highly pure α-Al$_2$O$_3$ pellet supplied by Setaram was used as the primary calibration standard. In addition, drop measurements were also made on OFHC grade copper samples [21], whose measured enthalpy increment values agreed to better than 2 % with the reported literature estimates [22]. A total of three experimental schedules covering the temperature range 400 K to 1273 K are conducted under highly pure argon (Iolar grade 2) atmosphere. Each schedule consists of a series of drop experiments performed at prefixed discrete temperature steps (approximately 25 K) so that the entire region of stability of the α-ferrite phase, besides some limited incursion into the γ-austenite domain, is covered in this study. In addition, a few more runs were performed at select temperatures in the neighbourhood of the transformation region to assess the extent of reproducibility and the typical scatter of enthalpy increment data. Apart from a few stray data points which are identified to be clear outsiders to the otherwise general trend, all other data points are used in the final analysis.

2.3 Accuracy of Transformation Temperature Data

Before proceeding with the presentation of the results, it is rather useful to bring into discussion some pertinent facts associated with the measurement accuracy of transformation temperature and enthalpy data using the drop calorimetry technique. First, it must be reiterated that the technique of drop calorimetry by virtue of its experimental design offers only discrete enthalpy increment data points at preselected temperature intervals. A continuous enthalpy curve as a function of temperature is not obtained by this technique. Hence, it is very likely that the exact or actual onset temperature of the phase transformation is either missed or only approximately located if the choice of the temperature interval between successive measurements is kept rather large. In this study, we have ameliorated this problem to some extent by maintaining approximately 25 K as the typical temperature interval between two consecutive drop experiments. Further, by beginning each successive experimental schedule with different starting temperatures, say from 400 K in the first run and from 425 K in the next one, etc., we could eventually gather multiple data points over the entire temperature range of interest with closer than 25 K temperature step. Thus, notwithstanding the fact that *discontinuous* drop calorimetry measurements generally yield only an approximate

estimate of the phase transformation temperature or domain, it is still possible to detect and trace the effect of the phase change on enthalpy in a definite manner using the drop technique by going in for many measurements conducted at close temperature intervals.

In addition, we may also note that the extent of temperature stability in each drop experiment is quite good in carefully conducted drop calorimetry studies. This is made possible by adopting a slow heating rate ($5 \, \mathrm{K \cdot min^{-1}}$) to reach the set temperature and further by ensuring a fairly long resident time at each isothermal holding step, we could achieve a temperature stability of ± 0.1 K under a steady high-pure argon (Iolar grade 2) flow. This level of thermal stability is vital to ensure a high level of precision or reproducibility in temperature measurement.

The other important technical issue concerning drop calorimetry data is the unavoidable scatter in the measured enthalpy values, especially in the high-temperature transformation range. It is our general experience that in properly conducted drop calorimetry measurements the different data points measured at nominally the same temperature do not reveal a scatter that is larger than 5 % of the measured enthalpy increment value [21]. Unfortunately for some of the data points especially in the transformation region, the observed scatter is somewhat larger. One source of reason is that successively dropped samples did *not* experience the same extent of phase transformation. This problem is ubiquitous to steel samples in which ensuring a very high level of sample homogeneity in a small mass is rather difficult. Although we could not do many drop measurements at each temperature, we did indeed carry out as many as three repeat runs at select temperatures with fresh samples while maintaining almost similar, if not exactly identical, experimental conditions. Only those data points that were clearly within the expected ± 5 % deviation band are taken into consideration. Thus, for example, if three successive drops yielded enthalpy increment values in the range $95 \, \mathrm{J \cdot g^{-1}}$ to $105 \, \mathrm{J \cdot g^{-1}}$, then a value of $100 \, \mathrm{J \cdot g^{-1}}$ is taken as the reliable average value of enthalpy for that particular chosen temperature. Some data points showed a deviation of more than $\pm 5 \, \mathrm{J \cdot g^{-1}}$ due to various reasons such as an incomplete phase transformation and dropped samples not fully penetrating into the bed or occasionally due to some mild oxidation, etc. These stray data points were not taken into account for the final analytical treatment.

Based on our previous experience obtained with stainless steel and pure copper samples [21], such procedure yielded quite satisfactory results. The transformation temperature reproducibility achieved in the three repeated drop experiments is in the range 2 K to 5 K (5 K is the maximum observed), and this has been convincingly established from the measurements done using pure iron (Aldrich Chemicals (Germany), less than 80 mass ppm of combined impurities).

It can be argued that in the case of a high-alloy steel with a comparatively poor thermal diffusivity, the scatter in the measured transformation temperature data can, in principle, be larger than that observed in the case of pure iron. This may be the case since the $\alpha \rightarrow \gamma$ transformation kinetics in steel is expected to be somewhat sluggish due to reasons of slow solutal diffusion. Thus, even for samples of the same mass, it would take a longer time to complete the phase change in steels as compared to pure iron. This point assumes considerable significance if the ΔT–t data collection time is kept short since, in which case, the full transformation enthalpy would not be recorded.

Strictly speaking, there is no fool-proof means of ascertaining this uncertainty in drop calorimetry measurements for a complex material like the present candidate. However, it is yet possible that a credible estimate of the transformation temperature and transformation enthalpy can be made by fixing an upper bound for the error bar based on experience obtained in measuring the transformation temperature of iron with 80 mass ppm carbon alloy. Based on this datum, we have *assumed* in this study a maximum uncertainty of ± 5 K in reporting transformation temperature values. We hasten to add that this should not be confused with the error associated with temperature measurements using the Pt(10 %Rh)/Pt thermocouple, which is estimated to be about $\pm 1\,K$. With this background information, we shall next enumerate the different features of the enthalpy increment versus temperature curve.

3 Results

3.1 Enthalpy Increment Versus Temperature Data

In Fig. 2, the measured enthalpy increment ($H_T - H_{298}$) values are plotted with respect to temperature, T. In order to avoid undue clutter arising from many very closely spaced data points, only the data corresponding to two typical runs (filled squares and circles) are shown in the figure. The smooth line connecting the data points serves to delineate the observed trend and certain distinct features of the enthalpy–temperature curve. In Table 1, the experimental enthalpy increment data are listed for select temperature intervals only. A quick perusal of Fig. 2 reveals that starting from 400 K the enthalpy exhibits a steady almost linear increase up to about 793 K. From this point, the enthalpy increment curve exhibits a distinct inflection with the subsequent onset of a nonlinear behaviour. The dotted line emanating from 793 K is drawn to indicate the probable extrapolated behaviour of enthalpy for the hypothetical case when the microstructure of the ferritic steel is assumed to remain unchanged during continued heating. In addition to this change of slope at 793 K, the presence of some other features in the otherwise smoothly increasing character of enthalpy is also clearly noticed in

Fig. 2 Temperature variation of the enthalpy increment values is shown. The *dotted line* at 793 K refers to the extrapolated linear behaviour of the ferrite phase if no microstructural changes accompany the heating process. The *dotted line* drawn from Ae$_1$ is the empirically extrapolated variation of the enthalpy sum of ferrite and austenite two-phase mixture
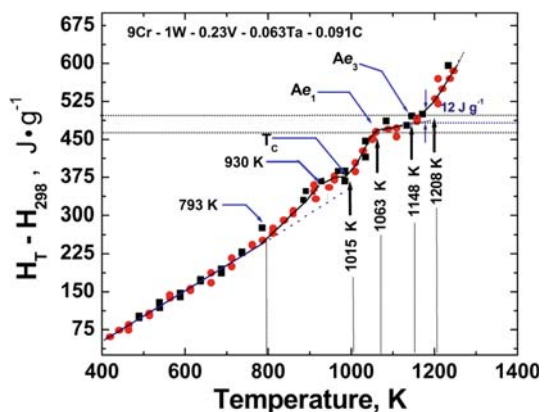
Table 1 Listing of the experimental enthalpy increment $\Delta°H = H_T - H_{298}$ values for the α-ferrite phase obtained in this study

Temperature (K)	Experimental enthalpy data $(J \cdot g^{-1})$	Fit enthalpy data $(J \cdot g^{-1})$	Error (%)	Temperature (K)	Experimental enthalpy data $(J \cdot g^{-1})$	Fit enthalpy data $(J \cdot g^{-1})$	Error (%)
464.1	77.2	74.8	−3.18	736.8	228.2	226.9	−0.55
464.3	77.3	84.6	8.68	761.6	242.1	243.0	0.35
489.3	90.9	101.7	10.67	761.9	242.3	241.9	−0.15
489.4	90.9	98.5	7.66	785.9	255.9	276.3	7.39
513.8	104.3	107.4	2.84	786.1	256.0	229.8	11.4
513.9	104.3	102.8	−1.48	812.0	271.1	275.5	1.62
538.7	118.1	118.6	0.440	811.0	270.5	265.8	−1.74
538.7	118.1	128.7	8.28	835.8	285.1	315.7	9.68
563.4	131.8	143.7	8.24	835.9	285.2	256.4	11.24
563.5	131.9	137.7	4.24	860.4	300.2	308.8	2.80
588.4	145.7	147.1	0.95	860.5	300.2	303.3	1.03
588.5	145.8	139.7	−4.36	885.4	315.9	296.7	−6.44
612.9	159.4	152.7	−4.36	885.5	316.0	302.0	−4.61
613.0	159.4	156.2	−2.06	910.2	332.2	347.2	4.32
637.3	172.9	171.2	−1.04	910.2	332.2	359.9	7.71
637.7	173.1	174.0	0.49	935.1	349.3	336.0	−3.95
662.5	186.9	187.4	0.30	935.2	349.4	395.1	11.58
662.5	187.0	167.8	11.39	959.5	367.1	377.0	2.64
687.2	200.6	195.0	−2.89	959.6	367.1	369.9	0.77
687.2	200.6	186.9	−7.31	984.7	386.4	387.7	0.33
712.1	214.4	200.0	−7.23	984.8	386.5	367.4	−5.19
712.3	214.5	216.5	0.92	1009.3	406.6	403.8	−0.69
736.8	228.2	228.5	0.12	1009.3	406.6	386.5	−5.20

The data are given only up to about 1000 K. For comparison, the values obtained by fitting the experimental data to Eq. 2 and the percentage deviation of the fit values from experimental estimates are also presented. The temperature and enthalpy values are rounded to one decimal place

Fig. 2. These points are marked by arrows in Fig. 2. Interpreting these inflections in the enthalpy–temperature curve in light of our recent findings on this steel using dynamic calorimetry [16], it can be said that these inflections or plateau-like characteristics in the enthalpy curve are indicative of the occurrence of phase transformations as they are also accompanied by finite changes in the enthalpy content. These are discussed in the following section.

3.2 On-Heating Phase Changes as Reflected by the Enthalpy–Temperature Curve

Starting from 400 K, the first major deviation from linearity is noticed around 793 K (520 °C). Since the starting microstructure in the quenched condition is one of a lath

martensite (Fig. 1) with a high dislocation density, this marked deviation from the linear enthalpy change is taken to be associated with the possible thermally activated relaxation of the *strained* martensite substructure. The available literature on the tempering physical metallurgy of 9Cr-steels supports this viewpoint [8]. With a further increase in temperature, this martensite relaxation is followed by the occurrence of a gentle plateau at around 930 K (657 °C). Since the martensite in low carbon (≤0.1 mass%) steel is basically one of *bcc*-ferrite that is supersaturated with carbon and further the temperature of 930 K (657 °C) is sufficient enough to bring about appreciable mobility of carbon atoms in the α-ferrite phase, it is possible that this second feature of the enthalpy curve is associated with the precipitation of $M_{23}C_6$ or M_7C_3 type carbides on prior austenite and inter-lath boundaries [8,23]. Thus, we attribute this second inflection feature in Fig. 2 to a carbide precipitation event.

Subsequent to carbide precipitation, the enthalpy rises steeply for a while before exhibiting another cusp at about 1015 (742 °C). Judging by our previous DSC results [16], this temperature corresponds to the Curie point T_C which marks the onset of the ferromagnetic-to-paramagnetic transition in the α-ferrite phase. The cusp at T_C is characteristic of only a small change in enthalpy and hence is not reflected sharply by present drop measurements. The magnetic transformation is closely followed by another region which persists up to 1063 K (798 °C). In fact, in the region bounded by 1063 K to 1148 K (798 °C to 875 °C), $\Delta°H$ changes in a steady fashion. The lower end of this range stands for the lower critical temperature designated as Ae_1 in Fig. 2. This temperature marks the onset of γ-austenite formation from α-ferrite + carbide mixture upon heating. The other temperature designated as Ae_3 stands for the upper critical temperature which signifies supposedly the completion of the austenite formation reaction. The region enclosed by Ae_1 and Ae_3 thus represents the $\alpha\text{-}ferrite+carbides \rightarrow \gamma\text{-}austenite$ three-phase inter-critical region [24]. Immediately after Ae_3, the enthalpy varies in an irregular manner for some small temperature interval, but from about 1208 K (935 °C) onwards it again registers a steadily increasing trend that is characteristic of the γ-austenite phase. The latter onset temperature varied somewhat among different experimental runs and in the present study it ranges from 1208 K to 1253 K (935 °C to 980 °C). This temperature is suggestive of the possible realization of homogeneous austenite following complete carbide dissolution in the high-temperature austenite [19]. It must be recalled that in high-alloy steels during continuous heating, the alloy carbide dissolution does not necessarily go to completion immediately following the completion of austenite reaction at Ae_3. The sluggish nature of carbide dissolution requires some small superheating above Ae_3 to facilitate the realization of homogeneous austenite [25].

3.3 Energetics of α-Ferrite + Carbide $\rightarrow$ γ-Austenite Phase Transformation

As discussed in the previous section and also brought out in our recent DSC study [16], the $\alpha \rightarrow \gamma$ phase change takes place in the temperature domain $Ae_1 \leq T \leq Ae_3$. Further, as seen in Fig. 2, the enthalpy also varies in a steady manner in this temperature interval. Since austenite formation is a nucleation and growth process, which involves a temperature-dependent change in both composition and phase fraction of

the respective constituents, a measurable heat effect follows as a consequence. Stating this in another manner, the observed total enthalpy in the Ae_1–Ae_3 domain derives both from the change in specific heat of the constituents as a function of temperature as well as from the enthalpy change ($\Delta^\circ H^{\alpha \to \gamma}$) associated with the $\alpha \to \gamma$ phase transformation. This point has been amply elaborated upon in our previous drop calorimetry studies on plain 9Cr-steels [19]. Hence, avoiding the repetition of a detailed explanation, we may write for H_T, the total enthalpy in the phase transformation regime ($Ae_1 \leq T \leq Ae_3$), the following expression,

$$H_T = H_0 + \int \{ (x_{\text{ferrite}} C_{p,\text{ferrite}}) + (x_{\text{carbide}} C_{p,\text{carbide}}) \\ + (x_{\text{austenite}} C_{p,\text{austenite}}) \} \, dT + \Delta^\circ H_{\text{tr}} \tag{1}$$

In the above expression, H_0 is the reference enthalpy at the transformation start temperature, taken after convention as Ae_1. The first contribution inside the curly brackets on the right-hand side of Eq. 1 stands for the mole fraction weighted sum of ferrite and austenite enthalpies. x_i denotes the phase (mole) fraction of the constituent i and $C_{p,i}$ its molar specific heat. It must be reiterated that in the temperature range $Ae_1 \leq T \leq Ae_3$, both x_i and $C_{p,i}$ are temperature dependent by virtue of the progress of the α-ferrite + carbide $\to \gamma$-austenite transformation. Thus, for example, at $T \leq Ae_1$, the austenite phase fraction (x_γ) equals zero; with increasing temperature, there is a gradual increase in its phase fraction, and as the Ae_3 temperature is approached, $x_\gamma \to 1$. Therefore, in the temperature range $T \leq Ae_1$, the observed total enthalpy is governed by the specific heats of α-ferrite and carbide only. But if we chose to ignore the small contribution from the carbide phase, the enthalpy variation is fully decided by the specific heat variation of α-ferrite alone. Similarly, for temperatures exceeding the Ae_3 point, the change in enthalpy is determined only by the specific heat of austenite; the small enthalpy effect due to austenite homogenization arising from the dissolution of any remaining trace of carbide is again discounted. In the intervening inter-critical region, the enthalpy is dictated by the dynamic course of the $\alpha \to \gamma$ transformation. It must be said that such a splitting of total enthalpy and hence C_p into two phenomenological components is driven by the necessity to understand the energetics of the $\alpha \to \gamma$ transformation in terms of simple and separable reaction steps. It may also be added that a rigorous calculation of the thermodynamics of a highly alloyed steel such as the present one requires specific information on phase fractions of ferrite, carbides and austenite as a function of temperature. More importantly, one also needs data on their individual specific heats so that a brute force calculation of $\Delta H_{\text{tr}}(T)$ using Eq. 1 can be attempted. While ferrite, austenite and carbide phase fractions as a function of temperature can be calculated through CALPHAD methodology [26], only scanty experimental data are available for their actual temperature-dependent specific heats $C_p^\alpha(T)$ and $C_p^\gamma(T)$. In view of such practical difficulties, we have chosen to simply extrapolate the enthalpy of ferrite from its region of stability into the inter-critical domain as well. A fair idea about the extent of progress of the $\alpha \to \gamma$ transformation or equivalently the volume fraction of ferrite remaining untransformed x_{ferrite}, at each temperature is obtained from our previous study of the transformation kinetics using differential

scanning calorimetry [16]. In this study, the fraction of austenite formed as a function of temperature in the transformation temperature domain is empirically estimated by adopting the Kolmogorov–Johnson–Mehl–Avrami model of diffusional transformation kinetics [16]. The area under the DSC peak after due calibration is taken to reflect the full phase transformation enthalpy, $\Delta°H_{tr}$. This value is estimated to be $14\,\text{J}\cdot\text{g}^{-1}$.

From Fig. 2, it can be estimated that the total enthalpy difference between the two limiting points Ae_3 and Ae_1 is about $35\,\text{J}\cdot\text{g}^{-1}$. As explained in Ref. [19], and also implicitly portrayed by Eq. 1, not the entire $35\,\text{J}\cdot\text{g}^{-1}$ is associated with the phase change effect. In fact, a good extent of it is associated with the weighted enthalpy sum from the untransformed fraction of ferrite and transformed austenite phase. This is actually the first term on the right-hand side of Eq. 1. This sum is simply *approximated* by extrapolating the enthalpy behavior from Ae_1, the transformation starting point up to the transformation finish temperature Ae_3. This extrapolation is graphically sketched as a dotted line in Fig. 2. The subtraction of this extrapolated value at Ae_3 from the total enthalpy difference of $35\,\text{J}\cdot\text{g}^{-1}$ yields about $12\,\text{J}\cdot\text{g}^{-1}$, and this value is taken to be the rough measure of the phase change enthalpy. As mentioned in Sect. 2.3, the measured total enthalpy difference between Ae_3 and Ae_1 is taken to be accurate to $\pm5\%$ in the present case. But the errors associated with the estimation of the fraction of austenite formed and also the uncertainty in C_p of ferrite and austenite will compound the final uncertainty only further. We have not made a systematic effort to evaluate this latter factor; but in spite of this, the value obtained for the transformation enthalpy is in good agreement with the estimate of $14\,\text{J}\cdot\text{g}^{-1}$ that is directly based on our previous differential scanning calorimetry measurements [16].

4 Discussion

4.1 Analytical Representation of $\Delta°H(T)$ Data

Since the enthalpy increment variation with temperature is basically nonlinear in nature, it is not possible to fit these data by a single functional form that is valid throughout the temperature range of this study. Further, we have not gathered adequate data points in the γ-austenite phase field to warrant a rugged analytical characterization of data in this regime. Therefore, the present analytical treatment of the data is restricted to the α-ferrite region only. The following empirical expression is used to fit the data in the temperature interval $400\,\text{K} \leq T \leq 1050\,\text{K}$ for the α-ferrite phase.

$$H_T - H_{298}/\text{J}\cdot\text{g}^{-1} = a/2\left(T^2 - 298^2\right) + b/3\left(T^3 - 298^3\right)$$
$$+ c/4\left(T^4 - 298^4\right) + d\ln\left(T/298\right)$$
$$- e'\left(T_C - T\right)/T_C \times \{\ln\left[\left(T_C - T\right)/T_C\right] - 1\}\}. \quad (2)$$

The above expression, basically empirical, is used from the point of view of convenience. Besides, it is consistent with the one that has been recently employed by us

for representing the $C_p(T)$ data obtained using differential scanning calorimetry [16]. Thus, consistent with Eq. 2, we get for $C_p(T)$ the following functional representation:

$$C_p^\alpha (T) /\text{J} \cdot \text{g}^{-1} \cdot \text{K}^{-1} = aT + bT^2 + cT^3 + d/T + e \ln [(T_C - T)/T_C]. \quad (3)$$

The last term in the above expressions stands for the magnetic contribution to the total enthalpy and specific heat, respectively, of the α-ferrite phase. T_C is the magnetic transformation temperature taken to be 1015 K for the present RAFM steel. A nonlinear least-squares regression of the enthalpy increment data to Eq. 2 yielded the following values for the fit coefficients:

$$\begin{aligned}
a &= 0.00463; \\
b &= -8.492 \times 10^{-6} \pm 4.9754 \times 10^{-7}; \\
c &= 4.8104 \times 10^{-9} \pm 5.5425 \times 10^{-10}; \\
d &= -122.17084 \pm 23.5675, \text{ and} \\
e' &= 0.0325.
\end{aligned} \quad (4)$$

It must be mentioned that the coefficient a is preset to the quoted value during the fitting procedure. While it is possible to treat this coefficient as a freely float parameter during fitting, it is found that fixing this quantity yielded a better fit ($R^2 = 0.98$); more importantly this gave, for C_p at 298 K, a value that agreed well with our previous differential scanning calorimetry-based estimate for the same sample [16]. In Table 2, the percentage deviation of the fitted $\Delta°H(T)$ values from the corresponding experimental ones is listed. It can be seen that Eq. 2 provides a satisfactory fit to the experimental data in the temperature range 400 K to 1050 K. In Table 3, the values of the fit coefficients appearing in Eq. 2 are compared for both the drop calorimetry-based direct enthalpy values and the indirect ones obtained from DSC-C_p data [16]. As can be seen from this table, there is a fair degree of correspondence between these two sets of coefficients, not withstanding the intrinsic differences in the manner the experiments are conducted in these two complementary calorimetry techniques. This aspect is addressed further in the following section.

Table 2 Listing of the values of fit coefficients in Eq. 2 used in the analytical representation of the temperature variation of the enthalpy increment ($H_T - H_{298}$/J $\cdot$ g^{-1}) data

| Coefficient	Drop data	DSC data
a	0.00463	$0.00491 \pm 0.14248 \times 10^{-3}$
b	$-8.49 \times 10^{-6} \pm 4.98 \times 10^{-7}$	$-8.47 \times 10^{-6} \pm 2.6 \times 10^{-7}$
c	$4.81 \times 10^{-9} \pm 5.54 \times 10^{-10}$	$4.66 \times 10^{-9} \pm 1.37 \times 10^{-10}$
d	-122.17 ± 23.5675	-171.90 ± 11.51
e	0.0325	$0.0325 \pm 1.25 \times 10^{-3}$
R^2	0.97	0.98

For comparison, the coefficients obtained for the DSC based enthalpy values are also listed

Table 3 Comparison of various transformation temperatures obtained in this study using drop calorimetry with the corresponding estimates based on differential scanning calorimetry [16]

Transformation	Drop calorimetry value (K)	DSC value (K)
Martensite relaxation	793	Not clearly observed
α-(martensite) $\rightarrow$ α-ferrite + carbide	930	937
Ferromagnetic α-ferrite $\rightarrow$ paramagnetic α-ferrite, T_C	1015	1018
α-Ferrite + carbide$\rightarrow$ γ-austenite + carbide	$Ae_1 = 1063$	$Ac_1 = 1104$
	$Ae_3 = 1148$	$Ac_3 = 1144$
γ-Austenite + carbide$\rightarrow$ γ-austenite (omogeneous austenite; completion of carbide dissolution)	1208–1253	

4.2 Comparison of Drop and Differential Scanning Calorimetry Data

As mentioned in Sect. 1, it is important to note that drop calorimetry is essentially a static or isothermal technique performed under near thermal equilibrium conditions. By maintaining the drop bed at several different closely spaced temperature intervals and carefully calibrating the instrumental sensitivity parameter at these temperatures, it is possible to trace the enthalpy increment variation with temperature in a *quasi-continuous* manner. The enthalpy increment data thus collected at discrete temperature increments can also be used to calculate the specific heat provided the temperature variation of enthalpy is satisfactorily represented by a suitable functional form. While a high level of accuracy in measuring the temperature as well as in ensuring its stability is possible in a drop calorimetry setup, it is however impossible to trace the enthalpy variation in a truly continuous manner, especially around regions of a phase transformation. This feature is in stark contrast to the dynamic or differential scanning calorimetry experiments, wherein continuous heating experiments are easily done, but at the cost of reduced accuracy in the temperature measurement and heat-flux calibration [27]. Thus, it is clear that the thermochemical data generated by these two techniques are bound to have certain differences that are germane to their respective designs. In Fig. 3, the practical manifestation of this aspect is graphically portrayed by comparing the C_p values obtained in this study (lower curve) with those of the dynamic calorimetry technique [16]. The DSC estimates (upper curve) are seen to be systematically higher than the equilibrium drop calorimetry values. In this case, the DSC experiments are conducted at a heating rate of $10 \, \text{K} \cdot \text{min}^{-1}$. In a strict sense, the DSC values need to be corrected for finite heating rate effects, so that a meaningful comparison can be made against the heating rate independent static drop calorimetry values. This is a very involved process to perform rigorously and in view of this we resorted to an empirical correction method based on our previous experience with the DSC-based measurements of the heat capacity of pure iron having 80 mass ppm of combined impurities [28]. Since fairly reliable and consistent values for the C_p of iron are available in the literature [29], this data set is used to calibrate the relative overes-
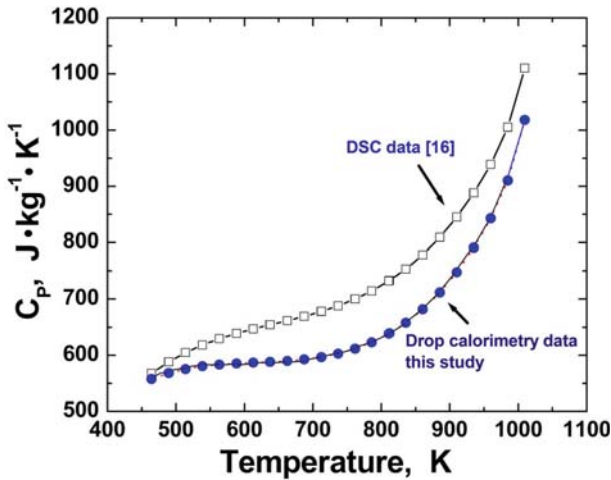
Fig. 3 Comparison of drop calorimetry-based C_p values (*lower line*) with the ones measured using DSC (*upper curve*) [16]

timation of our heat capacity measurement through the dynamic calorimetry method. This empirical temperature-dependent adjustment is applied to the DSC-based C_p data of the present RAFM steel as well [16].

In a similar manner, the various on-heating transformation temperatures obtained using DSC have also been corrected for the finite heating rate effects. These temperatures are compared with the present drop calorimetry-based values in Table 3. Although a fair degree of agreement is noticed among two sets of transformation temperatures, the value of Ae_1 is considerably less than that of Ac_1 obtained using DSC. It must be admitted that as mentioned elsewhere in this paper, there is some difficulty in precisely fixing the transformation onset point from merely studying the slope change or inflection associated with the enthalpy versus temperature curve; for as mentioned before, the drop experiments never trace the transformation event in a truly continuous fashion. It is quite likely that Ae_1 in this study is somewhat underestimated. However, this must also be weighed together with the well-known limitation that is intrinsic to DSC, in that the onset of the diffusional transformation solvus is always overestimated here resulting from the operation of finite heating rate effects [27]. Considering all these issues, we believe that the overall agreement between the drop and differential scanning calorimetry results for the transformation temperature is rather satisfactory.

4.3 General Points

As mentioned in Sect. 1, it must be reiterated that to the best of the present authors' knowledge not much data with regard to thermodynamic quantities of high chromium-reduced activation steels are available in the open literature [30–32]. In particular, we could not come across any drop calorimetry-based steady-state measurements of thermal quantities on this advanced fusion reactor material. However, in the recent past, there has been a renewed interest in the nuclear materials community in generating
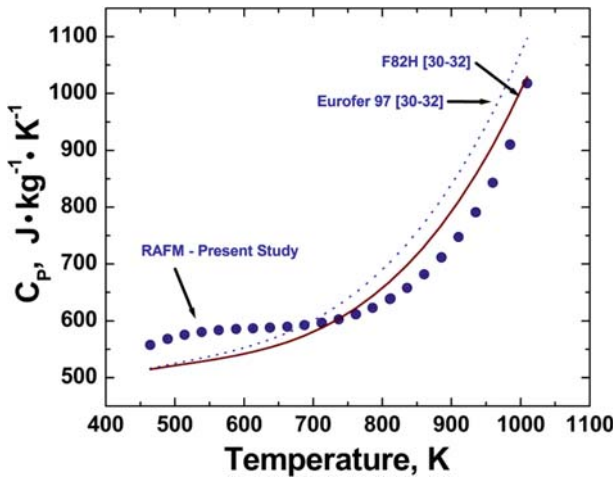
Fig. 4 Comparison of C_p of the reduced activation steel (RAFM) estimated in this study from present drop calorimetry enthalpy measurements with the literature data on Eurofer 97 and F82H [30–32]

a systematic property database on many emerging nuclear structural materials. Thus, two popular reduced activation steel grades, Eurofer 97 and F82H, have been extensively researched in the past and recommendations have already been drawn for their physical and mechanical properties [30–32]. The chemical compositions of these two steels are fairly similar (but not identical) to the RAFM steel used in this study. In Fig. 4, we have compared the recommended C_p–T data of both Eurofer 97 and F82H reduced activation steels with the present results. It is gratifying to note that the C_p values of the RAFM grade used in this investigation are in good accord with the reported ones.

A critical literature search for experimental phase equilibria-related information in this category of alloys does not make any explicit reference to the possible magnitude of the $\alpha \rightarrow \gamma$ transformation enthalpy. However, the present estimate of about $12 \, \mathrm{J \cdot g^{-1}}$ for this quantity appears reasonable when a comparison is made with respect to the transformation specific heat quoted for binary Fe–Cr alloys [33]. At present, a theoretical understanding of issues concerned with phase transformation energetics and kinetics in ferritic steels is handled mostly by phenomenological or CALPHAD-based approaches [14,26]. An adroit exploitation of this route requires the availability of reliable thermodynamic data. In this respect, it is hoped that the transformation temperature and $\alpha \rightarrow \gamma$ transformation enthalpy data generated in this study will be useful for developing a consistent thermodynamic dataset needed for the successful simulation studies of phase stability in high-chromium ferritic steels.

5 Conclusions

(i) Accurate enthalpy increment data as a function of temperature are measured using inverse drop calorimetry for tungsten and tantalum containing low carbon reduced activation steel.

(ii)   A critical comparison of the present isothermal enthalpy measurements with the results of our previous dynamic calorimetry studies has been made to reveal clearly the occurrence of various diffusional phase transformations that occur at high temperature.

(iii) The enthalpy data exhibited a nonlinear increase with temperature; distinct inflections are found at typical phase transformation temperatures. Estimates of various on-heating transformation temperatures have been determined. The detectable enthalpy change due to martensite relaxation has been found at 793 K. Further, the onset of carbide precipitation is found at 930 K. The magnetic transformation temperature T_C has been measured to be 1015 K. The Ae_1 and Ae_3 transformation temperatures have been determined to be 1063 K and 1148 K, respectively.

(iv)   The enthalpy increment data for the α-ferrite phase are fitted to a simple functional representation. This study suggests a value of $560 \, \mathrm{J \cdot kg^{-1} \cdot K^{-1}}$ for the specific heat at 450 K.

(v)   A value of $12 \, \mathrm{J \cdot g^{-1}}$ has also been obtained for the $\alpha \rightarrow \gamma$ phase transformation enthalpy.

References

1. S. Sharafat, G.R. Odette, J. Blanchard, J. Nucl. Mater. **386–388**, 896 (2009)
2. A. Danon, C. Servant, J. Nucl. Mater. **321**, 8 (2003)
3. R.L. Klueh, Int. Mater. Rev. **50**, 287 (2005)
4. V.K. Sikka, C.T. Ward, K.C. Thomas, Ferritic steels for high temperature applications, in *Proceedings of the ASM Conference on Production, Fabrication, Properties and Applications of Ferritic Steels for High Temperature Applications* (ASM, Metals Park, OH, 1983), pp. 65–84
5. S.J. Sanderson, *Interrelationships Between Mechanical Properties and Microstructure in a 9Cr 1Mo Steel, in Ferritic Steels for Fast Reactor Steam Generators* (BNES, London, 1978), pp. 120–127
6. J. Orr, S.J. Sanderson, An examination of the potential of 9Cr1Mo steel as thick section tube plates in fast reactors, in *Topical Conference on Ferritic Alloys for Use in Nuclear Technologies*, ed. by J.W. Davis, D.J. Michel (Metal Society of AIME, Warrendale, PA, 1984), pp. 261–267
7. W.L. Bell, T. Lauritzen, S. Vaidyanathan, Ferritics for breeder reactor In-core applications: a survey of alloys, properties and microstructure, in *Topical Conference on Ferritic Alloys for Use in Nuclear Technologies*, ed. by J.W. Davis, D.J. Michel (Metal Society of AIME, Warrendale, PA, 1984), pp. 113–124
8. M. Tamura, Y. Haruguchi, M. Yamashita, Y. Nagaoka, K. Ohinata, K. Ohnishi, E. Iitoh, H. Ito, K. Shinozuka, H. Esaka, ISIJ Int. **46**, 1693 (2006)
9. J. Hald, L. Korcakova, ISIJ Int. **43**, 420 (2003)
10. H. Finkler, M. Schirra, Steel Res. **61**, 328 (1996)
11. U.E. Klotz, C. Solenthaler, D.J. Uggowitzer, Mater. Sci. Eng. A **476**, 186 (2008)
12. F. Abe, Sci. Tech. Adv. Mater. **9**, 1 (2008)
13. V. Foldyna, J. Purmensky, Z. Kuban, ISIJ Int. **41**, S81 (2001)
14. H. Cerjak, P. Hofer, B. Schaffernak, ISIJ Int. **39**, 874 (1999)
15. R.L. Klueh, P.J. Maziasz, J. Nucl. Mater. **155–157**, 602 (1988)
16. S. Raju, B. Jeyaganesh, A.K. Rai, R. Mythili, S. Saroja, E. Mohandas, M. Vijayalakshmi, K.B.S. Rao, B. Raj, J. Nucl. Mater. **389**, 385 (2009)
17. M.J. Richardson, Application of differential scanning calorimetry to the measurement of specific heat. *Compendium of Thermophysical Property Measurement Techniques*, ed. by K.D. Maglic, A. Cezairliyan, V.E. Peletsky, vol. 2 (Plenum Press, New York, 1992), p. 519

18. Y. Zhu, J. Devletian, J. Mater. Sci. **26**, 6218 (1991)
19. S. Raju, B. Jeyaganesh, A. Banerjee, E. Mohandas, Mater. Sci. Eng. A **465**, 29 (2007)
20. A. Banerjee, S. Raju, R. Divakar, E. Mohandas, Int. J. Thermophys. **28**, 97 (2007)
21. A. Banerjee, S. Raju, R. Divakar, E. Mohandas, Mater. Lett. **59**, 1219 (2005) 2
22. M. Chase Jr. (ed.), *NIST-JANAF Thermochemical Tables, J. Phys. Chem. Ref. Data Monograph 9*, 4th edn. (ACS, Washington, DC, 1998)
23. J.M. Vitek, R.L. Klueh, Metall. Trans. **14**, 1047 (1983)
24. L. Karmazin, Mater. Sci. Eng. **100**, 201 (1988)
25. L.F. Alvarez, C. Garcia, V. Lopez, ISIJ Int. **41**, 599 (2001)
26. B.C. Schaffernak, H.H. Cerjak, Calphad **25**, 241 (2001)
27. E. Gmelin, S.M. Sarge, Thermochim. Acta **347**, 9 (2000)
28. B. Jeyaganesh, S. Raju, E. Mohandas, S. Murugesan, M. Vijayalakshmi, Int. J. Thermophys. **30**, 619 (2009)
29. Y. Chuang, R. Schmid, Y.A. Chang, Metall. Trans. **16**, 153 (1985)
30. A.-A.F. Tavassoli, A. Alamo, L. Bedel, L. Forest, J.M. Gentzbittel, J.W. Rensman, E. Diegele, R. Lindau, M. Schirra, R. Schmitt, H.C. Schneider, C. Petersen, A.M. Lancha, P. Fernandez, G. Filacchioni, M.F. Maday, K. Mergia, N. Boukos, Baluc, P. Spatig, E. Alves, E. Lucon, J. Nucl. Mater. **329–333**, 257 (2004)
31. A.-A.F. Tavassoli, J.W. Rensman, M. Schirra, K. Shiba, Fusion Eng. Des. **61–62**, 617 (2002)
32. K. Mergia, N. Boukos, J. Nucl. Mater. **373**, 1 (2008)
33. A.S. Normanton, R.H. Moore, B.B. Argent, Met. Sci. **10**, 207 (1976)